Effect of catch bonding on transport of cellular cargo by dynein motors

Anil Nair,[1] Sameep Chandel,[2] Mithun K. Mitra,[3] Sudipto Muhuri,[1] and Abhishek Chaudhuri[2]
[1]*Department of Physics, Savitribai Phule Pune University, Ganeshkhind, Pune 411007, India*
[2]*Indian Institute of Science Education and Research Mohali, Knowledge City, Punjab 140306, India*
[3]*Department of Physics, IIT Bombay, India*
(Received 16 February 2016; published 2 September 2016)

Recent experiments have demonstrated that dynein motors exhibit *catch bonding* behavior, in which the unbinding rate of a single dynein decreases with increasing force, for a certain range of force. Motivated by these experiments, we study the effect of catch bonding on unidirectional transport properties of cellular cargo carried by *multiple* dynein motors. We introduce a threshold force bond deformation (TFBD) model, consistent with the experiments, wherein catch bonding sets in beyond a critical applied load force. We find catch bonding can result in dramatic changes in the transport properties, which are in sharp contrast to kinesin-driven unidirectional transport, where catch bonding is absent. We predict that under certain conditions, the average velocity of the cellular cargo can actually increase as applied load is increased. We characterize the transport properties in terms of a velocity profile plot in the parameter space of the catch bond strength and the stall force of the motor. This plot yields predictions that may be experimentally accessed by suitable modifications of motor transport and binding properties.

DOI: 10.1103/PhysRevE.94.032403

I. INTRODUCTION

Motor-protein-driven transport of cellular cargoes along polar microtubule (MT) filaments is one of the principal mechanisms by which active long-distance transport is achieved within an eukaryotic cell [1,2]. This mechanism plays a vital role in keeping the cell spatially organized and maintaining the uneven distributions of the various cellular components [1,2]. While single-motor properties have been extensively studied, both in experiments and theory [3], a large class of cooperative transport processes depends critically on the interaction of various motors and their collective behavior, which can give rise to a whole new class of emergent phenomena [4–15].

The mechanism of this cooperative transport, however, remains an important open question. Experiments have revealed that unidirectional transport of cellular cargo involves the teamwork of motor proteins of a single type, e.g, the kinesin, dynein, and myosin family of motors, while bidirectional transport requires a team of oppositely directed kinesin and dynein motors [2,4,16]. While molecular architecture and transport properties of these different classes of motors are significantly diverse and different, existing theoretical studies have used the kinesin motor as a paradigm for motor-driven transport [8,9]. Crucially, the single-motor unbinding rate is modeled as an exponentially increasing function of force (slip bond) for both plus-end and minus-end directed motors [8,9]. However, recent experiments have shown that dynein unlike kinesin, exhibits *catch bond* behavior, where beyond a certain threshold force, the detachment rate of a single dynein from a MT filament decreases with increasing load force [4,17–19].

Catch bond behavior [20–22] has been observed in various biological protein receptor-ligand complexes, such as the complex of the leukocyte adhesion molecule P-selectin with the ligand PSGL-1 [23] and actin-myosin complex [24,25] as well as microtubule-kinetochore attachments [26]. Different mechanisms have been proposed for the catch bond [27–32] to varying degrees of success. In this paper, motivated by recent experimental and simulation studies of the dynein structure, we study the transport properties of cargo carried by several dynein motors, introducing a threshold force bond deformation (TFBD) model for the catch bond characteristics of dynein, consistent with experiments. We show that this cooperative transport, manifested in properties such as the average number of motors pulling on the cargo and the average velocity of the cargo, differs remarkably from kinesin-driven transport, where catch bonding is absent. We characterize these properties in terms of a velocity profile plot in the parameter space of the strength of the catch bond and the stall force of the motor, the force at which a single motor stops moving.

II. DYNEIN CATCH BOND

Cytoplasmic dynein has two heads that walk processively along the microtubule stalk in discrete steps. Each head has a globular region consisting of six AAA domains [19,33,34]. This globular region has two elongated structures emerging from it: the stalk, which binds to the microtubule, and the stem, which binds to the cargo [19]. It has been proposed that the globular head region contracts under applied load, which in turn causes tension to develop along the MT-binding stalk [19,33]. Beyond a certain critical load, this can lead to allosteric deformations in the receptor region of the dynein stalk and the ligand domain on the MT surface which lock them together (Fig. 1), resulting in a catch bond [19]. At low or intermediate loads, the catch bond cannot be activated and differential stepping is required to advance against the load [19]. Direct experimental evidence of catch bond behavior in dynein comes from recent *in vitro* and *in vivo* experiments on both single-molecule dynein detachment kinetics as well as collective behavior of a team of dynein motors [4,17,18]. The detachment rate of a dynein motor is found to initially increase, and then decrease with force beyond a critical threshold. At extremely large forces, we should eventually regain a slip bond, thus exhibiting a slip-catch-clip behavior over the entire force range.

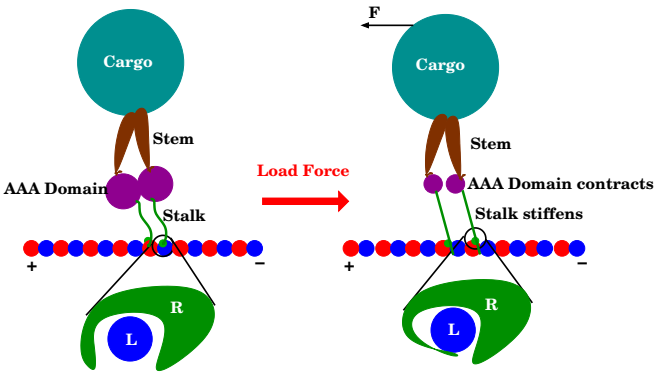

FIG. 1. Schematic representation of dynein walking on a MT filament, and catch bonding under applied load. The magnified region shows the MT binding domain of the dynein stalk, which can undergo a conformational change under applied load.

III. MODEL

We consider a cargo which is transported on a filament by N such dynein motors against a constant external load force F. The state of the cargo is characterized by the number of bound motors k ($0 \leqslant k \leqslant N$). Motors are irreversibly attached to the cargo but undergo attachment (detachment) to (from) the filament. With k bound motors, the rates of attachment and detachment are given by $\pi_k = (N-k)\pi_{\rm ad}$ and $\varepsilon_k = k\varepsilon$, respectively. Here, $\pi_0 (\equiv N\pi_{\rm ad})$ is the attachment rate for an unbound motor to the filament and ε is the detachment rate for a single bound motor. The load force is assumed to be shared equally by the k bound motors [8], so that each motor experiences a force $f = F/k$. The dynamics of the attachment-detachment process is given by the temporal evolution of the probability p_k of having k bound motors, expressed as the one-step master equation

$$\frac{dp_k}{dt} = \varepsilon_{k+1}p_{k+1} + \pi_{k-1}p_{k-1} - (\varepsilon_k + \pi_k)p_k. \qquad (1)$$

The corresponding master equation for the unbound vesicle ($k = 0$) is $dp_0/dt = \varepsilon_1 p_1 - \pi_0 p_0$, while for a vesicle with N bound motors, it is $dp_N/dt = \pi_{N-1}p_{N-1} - \varepsilon_N p_N$.

The bond deformation model proposes that catch bond behavior occurs by lowering the bound state due to force-induced deformation of the bond [32]. The deformation energy is given by $E_d(f) = \alpha[1 - \exp(-f/f_0)]$, where α characterizes the strength of the deformation energy expressed in units of k_BT and f_0 sets a force scale. Since *in vitro* dynein exhibits catch bond behavior above a threshold force $f > f_m$, we introduce the TFBD model with the deformation energy now given by

$$E_d(f) = \Theta(f - f_m)\alpha\left[1 - \exp\left(-\frac{f - f_m}{f_0}\right)\right]. \qquad (2)$$

The unbinding rate of a single dynein motor is then given by

$$\varepsilon(f) = \varepsilon_0 \exp[-E_d(f) + f/f_d], \qquad (3)$$

where the second term represents the usual slip contribution which exponentially grows with applied load. This TFBD model exhibits a *slip-catch-slip* behavior for a single-motor unbinding rate as a function of applied force on the motor. In a more general context, we also study the bond deformation (BD) model by setting f_m to zero in Eq. (3).

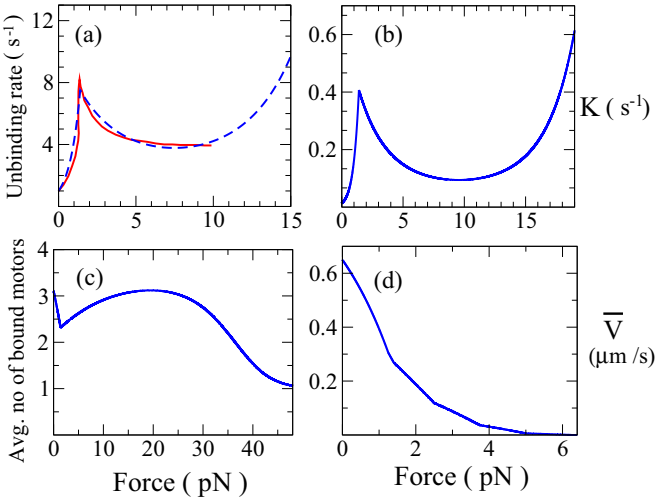

FIG. 2. (a) Variation of unbinding rate of a *single* dynein with constant load force (F): The red line corresponds to experiments from Ref. [17]. The dashed curve is obtained from the TFBD model with $\alpha = 68$, $f_o = 40.7$ pN, $f_m = 1.4$ pN, $f_d = 0.67$ pN, $f_s = 1.25$ pN [17], and $\varepsilon_0 = 1$ s^{-1} [17]. Transport properties of cargo carried by five dyneins as functions of F: (b) effective unbinding rate K vs F; (c) average number of attached motors vs F; and (d) average velocity vs F. For (b)–(d), the parameter values chosen are the same as in (a) with $\pi_{\rm ad} = 1.6$ s^{-1}[9] and $v_o = 0.65$ μm/s [9].

A cargo which is bound by k motors moves with a velocity v_k. With increasing load force, the velocity of the cargo is expected to decrease until it comes to a rest at some critical stall force f_s. The decrease is approximately linear [3,35–37] and is modeled by the usual force-velocity relation $v_k = v_0[1 - (F/kf_s)]$ where v_0 is the zero-force velocity for k bound motors, assumed to be independent of the number of bound motors.

The steady-state solutions to the master equation yield the probabilities for the unbound and the various bound motor states. The different transport properties are obtained after normalizing the probabilities with respect to the bound motor states alone [8].

IV. RESULTS

The unbinding rate of a single dynein as a function of the external load force was obtained in Ref. [17] by fitting experimentally observed detachment times in separate force regimes. We fitted our proposed TFBD model to determine the parameters corresponding to a single dynein. The TFBD model is able to capture the essential functional behavior as shown in Fig. 2(a) [17]. In fact, for load forces higher than those accessed by the experiment, we predict the usual slip behavior, a feature which is present in our TFBD model.

The parameters obtained from the fitting are next used to study how the catch bonding behavior exhibited by a single dynein affects the steady-state transport properties of cellular cargo that is being transported by N dynein motors. We consider $N = 5$ [38]. Figure 2(b) shows the effective unbinding rate of the cargo from the MT filament which

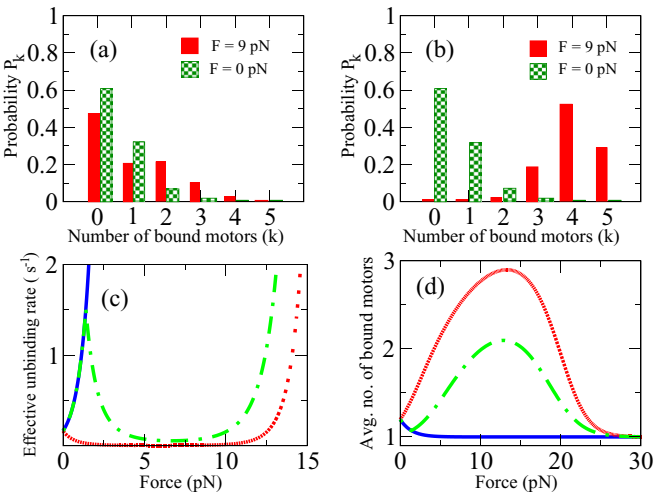

FIG. 3. Probability distribution for the number of bound motors in a system with $N = 5$ for the (a) TFBD and (b) BD models. Compared to the zero-force case (green crosses), where the probability distribution is peaked at zero bound motors and then decreases monotonically, for finite forces, both models show a nonmonotonic probability distribution, with the distribution peaking at larger k in the BD case. Panels (c) and (d) show the effective unbinding rate and the average number of bound motors as a function of force for a slip bond (solid blue line), as opposed to the TFBD (green dashed curve) and the BD (red dotted line) models. Data are for $\alpha = 20$ and $f_s = 2$ pN with $v_0 = 0.65$ μm/s [9], $\varepsilon_0 = 1.0$ s^{-1} [17], $f_0 = 7$ pN, $f_m = 1.4$ pN, $f_d = 0.67$ pN, and $\pi_{ad} = 0.1$ s^{-1}.

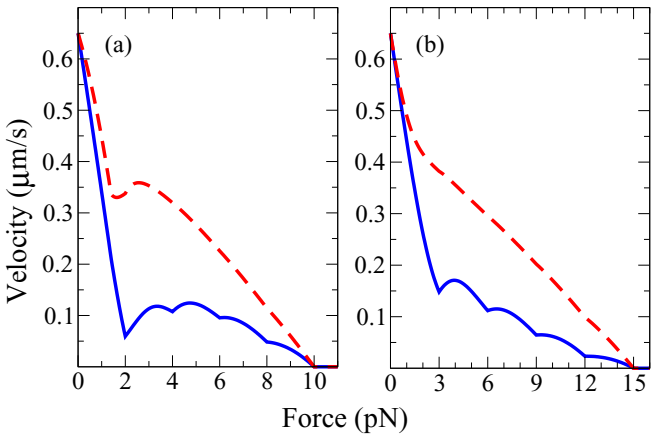

FIG. 4. Force-velocity curves: (a) TFBD model for two different binding rates, $\pi_{ad} = 0.1$ s^{-1} (solid blue curve) and $\pi_{ad} = 1.0$ s^{-1} (dashed red curve). The solid curve shows four velocity humps which reduces to a single-hump velocity profile on increasing π_{ad}. (b) BD model for $\pi_{ad} = 0.01$ s^{-1} (solid blue curve) and $\pi_{ad} = 0.1$ s^{-1} (dashed red curve). In this case, a four-hump profile reduces to a monotonically decreasing velocity profile on increasing π_{ad}. Data are for $N = 5$ motors with $v_0 = 0.65$ μm/s [9], $\epsilon_0 = 1.0$ s^{-1} [17], $\alpha = 35$, and $f_0 = 7$, $f_m = 1.4$, $f_d = 0.67$, and $f_s = 2$ pN.

qualitatively shows similar behavior to that of the single motor, increasing initially and then decreasing for forces up to about 10 pN, following which it again starts increasing with increasing load force. Figure 2(c) shows that the average number of attached motors also increases after an initial dip and finally decreases for forces larger than about 20 pN. The average number of bound motors exponentially approaches unity, since the normalization is with respect to bound motor states only. Figure 2(d) shows that the mean velocity of the cargo decreases monotonically with increasing load in this parameter regime.

Experimentally, it is known that the various motor properties can vary significantly for different classes of dynein motors. For instance, a *weak* dynein is known to have a stall force of $f_s = 1.1$ pN while for a *strong* dynein $f_s = 7$ pN [37]. We next explore the different *plausible* scenarios resulting from the ramifications of generic catch bond behavior, which has also been observed for myosin motors [24,25], by studying the transport properties both for the TFBD model ($f_m \neq 0$) and the BD model ($f_m = 0$). We shall focus on the variation of the transport properties resulting from changes in stall force f_s, binding rates π_{ad}, and catch bond strength α.

The effect of the catch bonding on the probability distribution of k bound motor state p_k is to shift the peak value of the distribution toward a higher number of bound motors for certain force ranges both for the TFBD model [Fig. 3(a)] and the BD model [Fig. 3(b)]. This shift results from the fact that when a larger number of motors is bound to the filament, the force on each motor is low enough that they are in the *catch* regime, resulting in a decrease of propensity of individual motors to detach from a filament in this state and hence a consequent increase in the probability of the states with higher numbers of attached motors. Conversely, when fewer motors bind to the filament, the load on each motor is higher, so that motors in this state are more likely to detach, and hence have a lower probability. This shifting of the peak of the probability distribution toward higher k states manifests as an increase in the average number of bound motors and a decrease in effective unbinding rates for a certain range of forces for both TFBD and BD models. This is shown in Figs. 3(c) and 3(d) and the behavior contrasts with the case of slip bonds where the effective unbinding rate monotonically increases and the average number of bound motors monotonically decreases with increasing load.

Next we consider the mean velocity profile of the cargo as a function of load force. Catch bond behavior manifests in a rather remarkable behavior for the velocity profile of the cargo: the mean velocity of the cargo can actually increase with increase in opposing load force for a certain range of parameter values, for both TFBD and BD models (Fig. 4). This unique behavior can be understood as a direct consequence of the catch bond effect, which tends to stabilize the bound motor states with higher attached motors which move with a higher velocity so that the average velocity of the cargo actually increases.

We systematically study the effect of variation of the stall force f_s and α by constructing a velocity-profile diagram with different regions characterized by the number of maxima of mean velocity in the force-velocity profiles. Figure 5 shows the resulting velocity diagrams for two different π_{ad} values each for the TFBD [Figs. 5(a) and 5(b)] and the BD Figs. 5(c) and 5(d)] models. The different regions correspond to different force-velocity profiles having multiple maxima. For sufficiently weak catch bond strength α, the force-velocity profile is such that the mean velocity always decreases for increasing load force, similar to the behavior in the absence

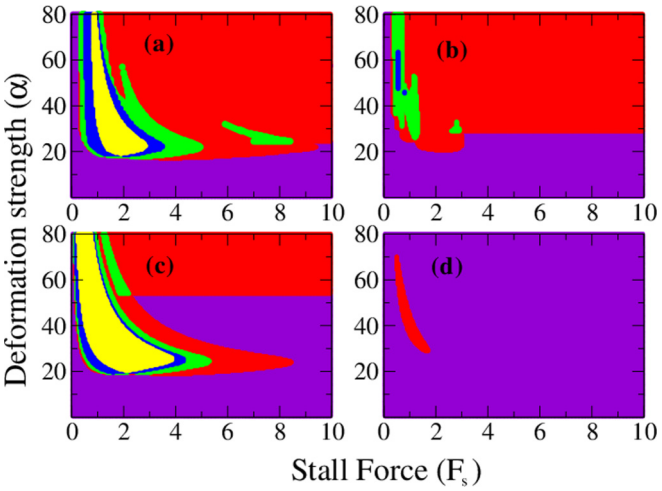

FIG. 5. Velocity diagrams in the α-F_s plane for the TFBD model with π_{ad} = (a) 0.1 and (b) 1.0 s^{-1}, and for the BD model with π_{ad} = (a) 0.01 and (b) 0.1 s^{-1}. The violet region corresponds to a monotonically decreasing force-velocity profile. The red, green, blue, and yellow regions correspond to velocity profiles with one, two, three, and four humps, respectively (see Fig. 4 for examples of individual velocity profiles). Parameter values are the same as in Fig. 4. Stall forces are in pN.

of catch bond. However, for both TFBD and BD models, increasing α and lowering f_s have the effect of modifying the force-velocity profiles in a manner that they have one or more maxima of the mean velocity as illustrated in Fig. 5. The parameter space explored is a plausible biological regime and in principle should be observable by suitable biochemical means which can alter the stall forces, catch bond strength, and/or binding rates of the motors to the filament.

V. CONCLUSION

We have proposed a model to capture the experimental results of catch bond behavior in a single dynein and studied the generic transport properties of a cargo driven by several such dynein motors. In contrast to canonical slip-bond models, our TFBD model for the catch bond has nontrivial consequences for the transport properties, in particular for the velocity profiles in response to applied loads, which should in principle be observable in experiments, and hence provide a testable prediction for our model. The more generic BD model also has similar dramatic differences in the transport properties, which might be relevant to other motor-driven systems. Indeed, even within our TFBD model, it is possible to find parameter regimes where the dissociation rate initially increases followed by a flat region ("slip-ideal" behavior) as reported in recent experiments on *in vitro* dynein [39]. The inclusion of additional but necessary complexities such as the effect of stochasticity [40], excluded volume, and hydrodynamic interactions could significantly alter the dynamics of the cargo and will be the subject of future study.

In summary, our work necessitates a reexamination of existing models of cellular cargo transport to take into account the catch bond mechanism described here. In particular, cooperative bidirectional cargo transport through the simultaneous action of oppositely directed motors (with one or both types of motor having a catch bond) is expected to have significantly different characteristics as compared to those described by existing theories, and will be discussed in a forthcoming publication.

ACKNOWLEDGMENTS

The authors would like to thank the organizers of the SMYIM conference, Pondicherry, where part of this work was done. M.K.M. acknowledges financial support from the Ramanujan Fellowship, Department of Science and Technology, India, and the IRCC Seed Grant, IIT Bombay. S.M. acknowledges DBT RGYI Project No: BT/PR6715/GBD/27/463/2012 for financial support. S.C. and A.C. acknowledge Department of Science and Technology, India, for financial support.

[1] B. Alberts *et al.*, *Molecular Biology of the Cell*, 4th ed. (Garland Science, New York, 2002).
[2] M. A. Welte, Curr. Biol. **14**, R525 (2004).
[3] J. Howard, *Mechanics of Motor Proteins and the Cytoskeleton* (Sinauer, Sunderland, 2001).
[4] A. K. Rai, A. Rai, A. J. Ramaiya, R. Jha, and R. Mallik, Cell **152**, 172 (2013).
[5] F. Jülicher, A. Ajdari, and J. Prost, Rev. Mod. Phys. **69**, 1269 (1997); F. Jülicher and J. Prost, Phys. Rev. Lett. **75**, 2618 (1995).
[6] T. Guérin, J. Prost, P. Martin, and J. F. Joanny, Curr. Opin. Cell Biol. **22**, 14 (2010).
[7] G. I. Menon, Physica A (Amsterdam) **372**, 96 (2006).
[8] S. Klumpp and R. Lipowsky, Proc. Natl. Acad. Sci. USA **102**, 284 (2005).
[9] M. J. I. Muller, S. Klumpp, and R. Lipowsky, Proc. Natl. Acad. Sci. USA **105**, 4609 (2008).
[10] F. Posta, M. Dórsogna, and T. Chou, Phys. Chem. Chem. Phys. **11**, 4851 (2009).
[11] O. Campás, Y. Kafri, K. B. Zeldovich, J. Casademunt, and J.-F. Joanny, Phys. Rev. Lett. **97**, 038101 (2006).
[12] T. Erdmann and U. S. Schwarz, Phys. Rev. Lett. **108**, 188101 (2012).
[13] V. Soppina, A. K. Rai, A. J. Ramaiya, P. Barak, and R. Mallik, Proc. Natl. Acad. Sci. USA **106**, 19381 (2009).
[14] D. Bhat and M. Gopalakrishnan, Phys. Biol. **9**, 046003 (2012).
[15] W. O. Hancock, Nat. Rev. Mol. Cell Biol. **15**, 615 (2014).
[16] V. Levi, A. S. Serpinskaya, E. Gratton, and V. Gelfand, Biophys. J. **90**, 318 (2006).
[17] A. Kunwar *et al.*, Proc. Natl. Acad. Sci. USA **108**, 18960 (2011).
[18] C. Leidel, R. A. Longoria, F. M. Gutierrez, and G. T. Shubeita, Biophys. J. **103**, 492 (2012).
[19] R. Mallik, A. K. Rai, P. Barak, A. Rai, and A. Kunwar, Trends Cell Biol. **23**, 575 (2013).
[20] O. V. Prezhdo and Y. V. Pereverzev, Acc. Chem. Res. **42**, 693 (2009).

[21] R. P. McEver and C. Zhu, Annu. Rev. Cell Dev. Biol. **26**, 363 (2010).
[22] S. Rakshit and S. Sivasankar, Phys. Chem. Chem. Phys. **16**, 2211 (2014).
[23] B. T. Marshall, M. Long, J. W. Piper, T. Yago, R. McEver, and C. Zhu, Nature **423**, 193 (2003).
[24] B. Guo and W. H. Guilford, Proc. Natl. Acad. Sci. USA **103**, 9844 (2006).
[25] A. Yamada, A. Mamane, J. Lee-Tin-Wah, A. D. Cicco, C. Prévost, D. Lévy, J. F. Joanny, E. Coudrier, and P. Bassereau, Nat. Commun. **5**, 3624 (2014).
[26] B. Akiyoshi *et al.*, Nature **468**, 576 (2010).
[27] E. Evans, A. Leung, V. Heinrich, and C. Zhu, Proc. Natl. Acad. Sci. USA **101**, 11281 (2004).
[28] V. Barsegov and D. Thirumalai, Proc. Natl. Acad. Sci. USA **102**, 284 (2005).
[29] D. Bartolo, I. Derényi, and A. Ajdari, Phys. Rev. E **65**, 051910 (2002).
[30] Y. V. Pereverzev, O. V. Prezhdo, M. Forero, E. V. Sokurenko, and W. E. Thomas, Biophys. J. **89**, 1446 (2005).
[31] E. A. Novikova and C. Storm, Biophys. J. **105**, 1336 (2013).
[32] Y. V. Pereverzev and O. V. Prezhdo, Phys. Rev. E **73**, 050902 (2006).
[33] R. Mallik, B. C. Carter, S. A. Lex, S. J. King, and S. P. Gross, Nature **427**, 649 (2004).
[34] M. P. Singh, R. Mallik, S. P. Gross, and C. C. Yu, Proc. Natl. Acad. Sci. USA **102**, 12059 (2005).
[35] N. J. Carter and R. A. Cross, Nature **435**, 308 (2005).
[36] S. Toba, T. M. Watanabe, L. Okimoto-Yamaguchi, Y. Y. Toyoshima, and H. Higuchi, Proc. Natl. Acad. Sci. USA **103**, 5741 (2006).
[37] M. J. I. Muller, S. Klumpp, and R. Lipowsky, J. Stat. Phys. **133**, 1059 (2008).
[38] It has been reported in Ref. [13] that for endosome transport four to eight dynein motors are involved.
[39] M. P. Nicholas, F. Berger, L. Rao, S. Brenner, C. Cho, and A. Gennerich, Proc. Natl. Acad. Sci. USA **112**, 6371 (2015).
[40] S. Klein, C. Appert-Rolland, and L. Santen, Europhys. Lett. **111**, 68005 (2015).